THE JOURNAL OF PHYSICAL CHEMISTRY B

Article

pubs.acs.org/JPCB

Utilizing the Dynamic Stark Shift as a Probe for Dielectric Relaxation in Photosynthetic Reaction Centers During Charge Separation

Zhi Guo,*[,†,§] Su Lin,[†,‡] and Neal W. Woodbury*[,†,‡]

[†]The Biodesign Institute at Arizona State University, [‡]Department of Chemistry and Biochemistry, and [§]Department of Physics, Arizona State University, Tempe, Arizona 85287-5201, United States

Supporting Information

ABSTRACT: In photosynthetic reaction centers, the electric field generated by light-induced charge separation produces electrochromic shifts in the transitions of reaction center pigments. The extent of this Stark shift indirectly reflects the effective field strength at a particular cofactor in the complex. The dynamics of the effective field strength near the two monomeric bacteriochlorophylls (B_A and B_B) in purple photosynthetic bacterial reaction centers has been explored near physiological temperature by monitoring the time-dependent Stark shift during charge separation (dynamic Stark shift). This dynamic Stark shift was determined through analysis of femtosecond time-resolved absorbance change spectra recorded in wild type reaction centers and in four mutants at position M210. In both wild type and the mutants, the kinetics of the dynamic Stark shift differ from those of electron transfer, though not in the same way. In wild type, the initial electron transfer and the increase in the effective field strength near the active-side monomer bacteriochlorophyll (B_A) occur in synchrony, but the two signals diverge on the time scale of electron transfer to the quinone. In contrast, when tyrosine is replaced by aspartic acid at M210, the kinetics of the B_A Stark shift and the initial electron transfer differ, but transfer to the quinone coincides with the decay of the Stark shift. This is interpreted in terms of differences in the dynamics of the local dielectric environment between the mutants and the wild type. In wild type, comparison of the Stark shifts associated with B_A and B_B on the two quasi-symmetric halves of the reaction center structure confirm that the effective dielectric constants near these cofactors are quite different when the reaction center is in the state $P^+Q_A^-$, as previously determined by Steffen et al. at 1.5 K (Steffen, M. A.; et al. *Science* **1994**, *264*, 810−816). However, it is not possible to determine from static, low-temperature measurments if the difference in the effective dielectric constant between the two sides of the reaction center is manifest on the time scale of initial electron transfer. By comparing directly the Stark shift dynamics of the ground-state spectra of the two monomer bacteriochlorophylls, it is evident that there is, in fact, a large dielectric difference between protein environments of the two quasi-symmetric electron-transfer branches on the time scale of initial electron transfer and that the effective dielectric constant in the region continues to evolve on a time scale of hundreds of picoseconds.

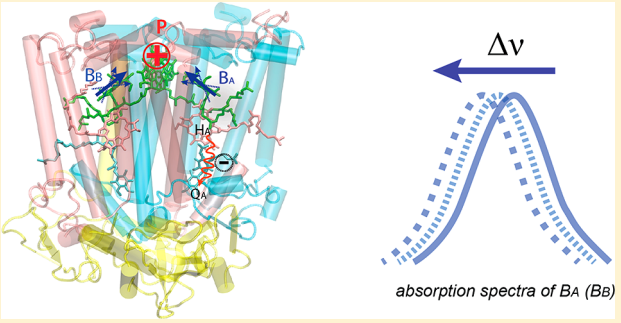

INTRODUCTION

Molecular systems exposed to external electric fields can undergo changes in the energy of one or more electronic states that manifest themselves as a shift of the coresponding absorbance transition (the Stark effect[2,3]). This provides information not only about the nature of the transitions themselves (dipole moments, polarizability) but also about the dielectric nature of the local environment. As a result, a considerable body of literature has accumulated on the measurement and treatment of Stark effects in biomolecules and organic molecules.[4−15] Photosynthetic reaction centers provide a particularly interesting system for these kinds of measurements because the light-driven reactions themselves generate strong, oriented electric fields in the complex. The reaction centers of *Rhodobacter (Rb.) sphaeroides* have been particularly well studied in this regard (refs 1, 16, and 17). In these reaction centers, charge separation is initiated by excitation of a dimer of bacteriochlorophyll molecules (P) forming the excited state P*. Subsequently, an electron is transferred along a series of cofactors (the so-called A-side or L-side cofactors in the quasi-symmetric reaction center complex) first to a monomeric bacteriocholorophyll (B_A) in ∼3 ps, then to a bacteriopheophytin (H_A) with a time constant of ∼1 ps, then to the first of two quinones (Q_A) in about 200 ps, and finally to the second quinone (Q_B) on the microsecond time scale (for review, see refs 18 and 19). The B-side cofactors, B_B, H_B, and Q_B, are symmetrically related by an approximate C-2 axis to their A-side counterparts (the detailed protein environment is different), but other than the final transfer

Special Issue: Rienk van Grondelle Festschrift

Received: April 16, 2013
Revised: June 12, 2013
Published: June 25, 2013

from Q_A to Q_B, the B-side cofactors are not thought to be involved in normal charge separation. This functional asymmetry arises from differences in the protein environment around the otherwise identical cofactors.

When charge separation takes place in the reaction center, the intramolecular electric field created induces shifts in the ground-state absorption bands of neighboring cofactors.[1,4,6,9,20] In general, the peak transition frequency ν_{max} associated with a particular absorbance band shifts as a function of the external field $\vec{E}$

$$\Delta\nu(\vec{E}) = -\overrightarrow{\Delta\mu}\cdot\vec{E} - \frac{1}{2}\vec{E}\cdot\Delta\alpha\cdot\vec{E} + \ldots \quad (1)$$

Here $\overrightarrow{\Delta\mu}$ and $\Delta\alpha$ are the difference permanent dipole moment (between the ground state and excited state) and the difference polarizability, respectively. The difference absorption spectrum can further be expanded as a Taylor series in powers of $\Delta\nu$,[4,9,20,21] that is

$$\varepsilon(\nu, \boldsymbol{E}) - \varepsilon(\nu, 0) = -\left(\frac{\partial\varepsilon(\nu, 0)}{\partial\nu}\right)\frac{\boldsymbol{E}\cdot\Delta\mu}{h} - \left(\frac{\partial\varepsilon(\nu, 0)}{\partial\nu}\right)\frac{\Delta\alpha|\boldsymbol{E}|^2}{h} + \frac{1}{2}\left(\frac{\partial^2\varepsilon(\nu, 0)}{\partial\nu^2}\right)\frac{|\Delta\mu|^2|\boldsymbol{E}|^2}{h^2} + \ldots \quad (2)$$

In reaction centers, the absorbing molecule is a bacteriochlorophyll, and the field induced via charge separation is uniform relative to the orientation of the transition dipole of the absorption transition being probed. Under these conditions, one would expect the first-order terms to dominate,[9,22] and Lao et al. have shown previously in reaction centers that for the monomeric bacteriochlorophylls, the excited state polarizability, $\Delta\alpha$, is small.[23] As a result, for the situation described here, eq 2 can be simplified to a good approximation to only the first term, resulting in a simple linear relationship between the spectral change and the electric field.

One of the more interesting questions that arises in looking at the bacterial reaction center structure is whether differences between the dielectric environment surrounding cofactors on the A and B sides are substantially different and what functional role this might play in the asymmetry of electron transfer between the two potential pathways. Detailed studies of Stark effects using high-resolution, low-temperature absorbance spectroscopy of *Rb. sphaeroides* reaction centers have been performed[6,20,24−26] and have been used to compare the protein environment of the A-side (L-side, active branch) cofactors to the B-side (M-side, inactive branch) cofactors in the reaction center complex.[1] These studies concluded that there was a substantial difference in the dielectric environment felt by A- and B-side cofactors, in particular, B_A and B_B, when the reaction centers were photopumped into the long-lived $P^+Q_A^-$ state. This is significant as these cofactors are presumably involved in the initial symmetry-breaking reaction. Of particular interest, the apparent dielectric constant on the A-side, calculated by comparing the B_A ground-state absorbance band shift to what one would expect in vacuum, was much larger than that on the B-side, suggesting that the protein environment of B_A has evolved to stabilize charge separation to a greater extent than the environment of B_B on the inactive B-side. Subsequently, low-temperature Stark measurements were extended to earlier times and charge-separated intermediates.[17] These measurements were performed largely for the purpose of understanding coherence effects in the system[17] but also provided time-resolved data for the shift in the ground-state band of B_A over the first few picoseconds. Not surprisingly, the band shift associated with B_A is considerably greater when reaction centers are in the state $P^+H_A^-$ on the picosecond time scale compared to the band shift in the presence of a steady-state population of $P^+Q_A^-$ produced by continuous illumination. $P^+H_A^-$ places B_A directly between a positive and negative charge, increasing the applied field strength. The effective dielectric constants reported in the region near B_A are similar in the two studies.[1,17]

All of the previous work was performed at cryogenic temperatures (1.5 or 15 K).[1,17] Under these conditions, protein movement is severely constrained, and thus, the part of the dielectric response to charge separation that depends on protein motion will be greatly decreased or at least slowed down. In addition, the dynamic studies performed were restricted to the primary electron-transfer reaction and did not follow the field changes that occur as the electron is transferred from H_A^- to Q_A. Here, dynamic Stark shift measurements of the lowest-energy (Q_Y) transitions of B_A and B_B are performed at room temperature, where protein motion can play a major role in dielectric relaxation and measurements are made through the time course of electron transfer from P* to Q_A with subpicosecond time resolution. In addition, mutants shown previously to affect the B_A local environment and to alter both the time course of electron transfer to H_A and subsequent transfer to Q_A are explored, and their kinetics of dielectric relaxation is compared to that of wild type.

MATERIALS AND METHODS

Mutant Preparation and Reaction Center Protein Isolation. The tyrosine at position M210 in wild type *Rb. sphaeroides* reaction centers was replaced with four other amino acids, generating the mutations M210YA, M210YD, M210YF, and M210YW using methods described previously.[27−29] Reaction center isolation and purification was also performed as previously described.[30] The reaction center samples were suspended in 50 mM tris-HCl buffer (pH 8.0), 0.025% LDAO detergent, and 1 mM EDTA for transient absorbance measurements. Quinone removal to generate Q_A-depleted reaction center samples followed published methods.[31]

Spectroscopic Measurements. The femtosecond pump−probe system used to measure transient absorption changes has been described.[29] In brief, the laser pulses were generated at a reptition rate of 1 kHz with 130 fs duration at 800 nm using a regenerative amplifier system based on a titanium:sapphire laser (Millennia, Tsunami, Spitfire, Spectra-Physics lasers). About 70% of the beam power was used to pump the infrared optical parametric amplifier (OPA-800C, Spectra-Physics), and the remaining 30% was used to generate the white light continnum for the probe beam. Excitation at 860 nm was obtained by second-harmonic generation of the idler beam from the optical parametric amplifier. White light pulses used as the probe beam were generated by focusing 800 nm pulses onto a 3 mm sapphire plate followed by pulse compression using a pair of prisms (CVI). The polarization of the excitation beam and the probe beam was set to a magic angle (54.7°) with respect to each other. The probe light was dispersed by a spectrograph and detected by a CCD detector over the spectral range from 680 to 980 nm, with a spectral resolution of 2.4 nm. Samples were placed between two quartz plates sealed in a wheel (1.2 mm path length) that rotates to avoid accumulating long-lived

dx.doi.org/10.1021/jp4037843 | J. Phys. Chem. B 2013, 117, 11383−11390

$P^+Q_A^-$. The translation stage used as part of the delay line for the kinetics measurements allows up to a 6 ns delay to be introduced between the pump beam and the probe beam. All measurements were performed at room temperature.

Data Analysis. The spectroscopic analysis was restricted to the cofactor transitions in the Q_Y transition region of the spectrum and specifically the primary electron donor (P) band at 865 nm, the monomeric bacteriochlorophyll transitions (B_A and B_B) near 800 nm, and the bacteriopheophytin transitions (H_A and H_B) near 760 nm. The analysis procedure consists of three steps (Figure 1).

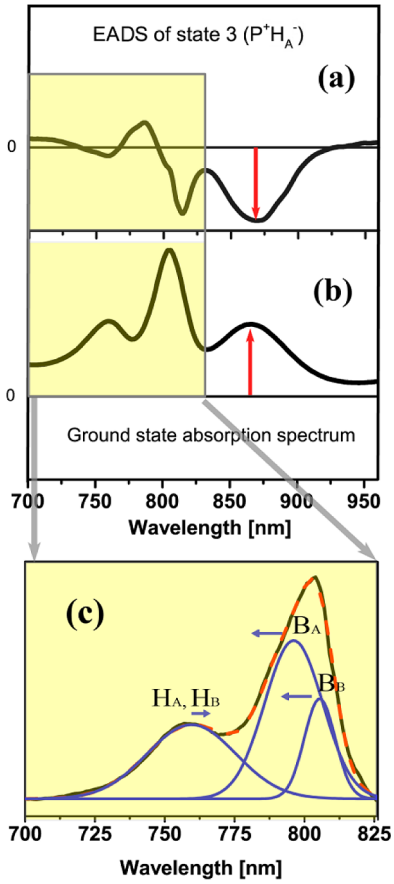

Figure 1. The construction of an absolute absorption spectrum at a particular time during photoinduced charge separation starting from an evolution-associated difference spectrum (EADS) derived from a time versus wavelength transient absorbance measurement (see text). The ground-state absorption spectrum (b) and the difference absorption spectrum at a particular time (a) are normalized to the amplitude of the P band (indicated by the red arrows). Addition of these two normalized spectra results in the absolute time-dependent absorption spectrum (c). The absolute absorption spectrum then is fitted with three Gaussian bands to reveal the positions of the B_A and B_B individual absorbance bands as a function of time. Comparison of the spectral positions of these bands over time allows determination of the band shifts (blue arrows, detailed in text).

In the first step, global analysis was performed using Glotaran software[32] on the entire set of time-resolved spectra and modeled in terms of a series of sequential states (A → B → C → ...). The resulting, so-called, evolution-associated difference spectra (EADS) were used for this analysis simply as a representation of the raw spectra in order to reduce spectral noise in subsequent calculations (see below); they do not necessarily individually correspond to physically meaningful states. Five to seven components (depending on the mutant) were required to fit the time-resolved spectral data in the Q_Y region adaquately. The first one or two EADS were dominated primarily by P* judging from their EADS profiles and time constants. Those EADS were not included in the subsequent calculations because the Stark shifts in the excited state were small, and the stimulated emission from P* would complicate the spectral fitting described below. The remaining four to six EADS (depending on the sample), with decay lifetimes between 2 ps and 77 ns, were dominated by charge-separated states and were used in the dynamic Stark shift analysis described below.

In the second step, each of the EADS was scaled so that the amplitude of the P band bleaching at 865 nm matched that of the ground- state absorption band of P at the same wavelength. By then summing each EADS individually with the ground-state spectrum, a set of time-dependent absolute absorbance spectra were generated. Note that normalization of the individual EADS on each time scale removes any effect of yield loss due to recombination to the ground state (which occurs in some of the mutants used in this study) because only the reaction centers in the state P^+ on that time scale are effectively considered in the construction of the absolute time-resolved spectra.

In the third step, each time-resolved absolute absorption spectrum, constructed from a selected EADS, was used to calculate band shifts of B_A and B_B ($\Delta\nu_{B_A}\Delta\nu_{B_B}$). As in Steffen et al.,[1] this was performed via Gaussian spectral fitting. Steffen et al. used two Gaussian bands to fit each cofactor absorption band in the 1.5 K absorbance spectra that they measured. Here, all spectra were recorded at room temperature, and the decreased spectral structure at this temperature required only a single Gaussian function to fit either the B_A or B_B absorption bands. Previous studies have suggested that B_B absorbs at lower energy than B_A.[33] The Gaussian bands derived from the fits were assigned accordingly, resulting in a B_B absorption band strength significantly lower than that of B_A, again in accordance with past work.[1] Performing the Gaussian spectral fitting on a series of EADS in this way is analogous in some respects to performing a global analysis on the time-resolved spectra. In this case, the constrained global parameters are the widths of the Gaussian absorption bands (i.e., the widths of each band are allowed to vary during the fit but assumed to be the same for all EADS included in the fit, while the amplitudes and peak positions of each Gaussian band are free to change between EADS). A complete time dependence of the B_A (or B_B) band shift $\Delta\nu(t)$ can then be calculated by weighting the spectral shift value determined from each EADS by the time-dependent coefficient associated with the EADS

$$\Delta\nu(t) = \sum_i C_i(t)\cdot\Delta\nu_i^{\mathrm{EADS}}(t) \tag{3}$$

where $C_i(t)$ is the population of ith EADS state at time t (given by its kinetics) and $\sum_i C_i(t) = 1$. Because only EADS associated with charge-separated states are included, the time course of the Stark shift is associated with the formation and decay of charge separation. Contributions to the shift from the excited state are expected to be small. Note also that for this analysis, B_A is presumed to be predominantly in its ground state throughout charge separation (a requirement if it is to be a reliable probe of the surrouding field). One might be concerned that transient

dx.doi.org/10.1021/jp4037843 | J. Phys. Chem. B 2013, 117, 11383−11390

formation of B_A^- during charge separation would complicate the analysis. However, for the conditions and samples tested, the B_A^- population is calculated to be below 20% even at the peak of its formation, which lasts less than 1 ps. Thus, electron transfer via B_A should not significantly affect the dynamics presented.

RESULTS AND DISCUSSION

The dynamic Stark effects in wild type reaction centers and several mutant reaction centers were determined. In particular, the mutants included replacement of the tyrosine residue at M210 with alanine (M210YA), aspartic acid (M210YD), tryptophan (M210YW), and phenylalanine (M210YF). Past work[29,34−37] has shown that these mutations do not significantly change the reaction center cofactor composition or its absorption spectrum, and there is no evidence suggesting that these mutations greatly alter the balance between electron transfer on the A versus B cofactor branches of the reaction center. However, the proximity to B_A makes it likely that these mutations perturb the dielectric environment in that region, and there is evidence that at least one of these, M210YD, differentially alters both electron transfer and protein relaxation processes in the $P^* \rightarrow P^+H_A^-$ and $P^+H_A^- \rightarrow P^+Q_A^-$ reactions.[29]

B_A Stark Shift. Figure 2a shows the time dependence of the Stark shift associated with the ground-state spectral band of B_A in wild type reaction centers (see the Materials and Methods section for details of the analysis) compared to the development and decay of the state $P^+H_A^-$, which is monitored by observing the H_A ground-state bleaching at 545 nm (the later signal is inverted and normalized for comparison to the Stark shift). In principle, the Stark signals from B_A should reflect the apparent field strength at B_A and follow the kinetics of $P^+H_A^-$ formation quite closely. As can be seen in Figure 2, the Stark shift and the initial electron transfer do, in fact, correspond kinetically, a fact that is consistent with the kinetic analysis of Vos et al. at cryogenic temperature (though they did not perform a direct comparison).[17] The coincidence between the kinetics of electron transfer and the B_A Stark shift kinetics imply that the protein dielectric relaxation is slow compared to kinetics of electron transfer (i.e., protein dynamics does not alter the effective dielectric constant appreciably on this time scale).[38−40] The formation of $P^+H_A^-$ generates a field not present in the ground state, and as the population of this state increases, a larger and larger fraction of the reaction centers shows the corresponding shift in the B_A transition. As discussed in the Supporting Information, the early time shift contains kinetic information about both the $P^* \rightarrow P^+B_A^-$ reaction and the $P^+B_A^- \rightarrow P^+H_A^-$. In particular, the electron-transfer kinetics of the two initial reactions of the mutants vary by as much as an order of magnitude, and these kinetics correspond to the dynamic Stark shift in predictable ways (Figure S4, Supporting Information).

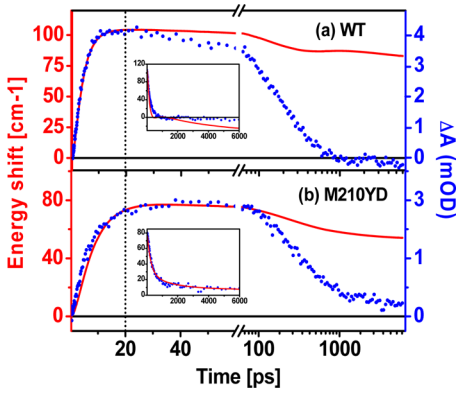

Figure 2. Comparison of the time-dependent B_A Stark shift (red lines) with the electron-transfer kinetics measured at 545 nm (blue dots; the bleaching signal of H_A has been inverted for comparison) over a 6 ns time window. Note that the time axes are linear up to 60 ps and then logarithmic to 7 ns. Both kinetic traces are normalized at the maximum. (a) Wild type reaction centers. (b) M210YD reaction center mutant. Insets: The same data plotted on an entirely linear time scale in such a way that the Stark shift trace (red) and the electron-transfer trace (blue) are normalized at 20 ps and 1 ns for comparison. All measurements were performed at pH 8.0 and room temperature.

In the M210YD mutant (Figure 2b), the formation of $P^+H_A^-$ is slower than that of wild type, roughly 7 ps[29] (see Figure S4 (Supporting Information) for the kinetics of the Stark shift in the other mutants). Unlike wild type, the B_A Stark shift in this mutant grows in significantly more slowly than H_A^- is formed (this phenomenon is also observed for M210YW, a slow charge separation mutant; see Figure S4, Supporting Information). In other words, rather than the shift occurring as charge separation takes place, it lags behind it; the maximum effect of charge separation on the field strength at B_A does not appear instantateously relative to the time scale of the charge separation reaction.

One way to rationalize a difference in the time dependence of the expression of the B_A Stark shift and the population of the $P^+H_A^-$ charge-separated state is to suppose that the effective dielectric environment near B_A in the M210YD reaction centers changes after charge separation due to protein dynamics on this time scale. The fact that the effective field strength on B_A lags behind the electron-transfer reaction implies that the shift of the B_A band that takes place during charge separation continues afterward, so that the time course of the overall, normalized shift appears slightly longer. This could be explained in terms of a local reorganization of the protein environment on the picosecond time scale, enhancing the local field and accentuating the B_A band shift. An enhancement of the field is somewhat counterintuitive; normally, dielectric relaxation in response to a field results in a decrease, rather than an increase, in field strength. However, in complex systems such as this, field changes need not be uniform, and this measurement only samples the field at a single region. In addition, past work has suggested that a fast equilibrium between $P^+B_A^-$ and $P^+H_A^-$ (~1 ps) takes place in M210YD at early times,[29] and this could result in rather different relaxation of the B_A environment, over several picoseconds, than would occur in a pure $P^+H_A^-$ state. Such a scenario is consistent with the previously reported fast charge recombination of $P^+H_A^-$ in this mutant, which presumably takes place via substantial thermal repopulation of $P^+B_A^-$.[29]

For both the wild type and the M210YD mutant reaction centers, the decay of the dynamic Stark shift on the 100 ps to nanosecond time scale involves multiple phases, and the majority of the band shift remains after several nanoseconds. The faster decay phase of the B_A dynamic Stark shift takes place in hundreds of picoseconds, as does the $H_A^- \rightarrow Q_A$ electron-transfer reaction. However, in wild type reaction centers, the band shift proceeds more rapidly (~130 ps time constant) than the actual charge separation reaction (~200 ps time constant) (Figure 2, inset). Wavelength-dependent kinetics of the $H_A^- \rightarrow Q_A$ reaction have been observed previously and were explained

dx.doi.org/10.1021/jp4037843 | J. Phys. Chem. B 2013, 117, 11383−11390

Table 1. Stark Shift Associated with the Two Electronic States, $P^+H_A^-$ and $P^+Q_A^-$ for Each of the Mutants Studied in This Work[a]

mutant name	B_A ($P^+H_A^-$)	B_A ($P^+Q_A^-$)	B_B ($P^+H_A^-$)	B_B ($P^+Q_A^-$)
WT	104 ± 4 (507−660[c])	83 ± 4 (367[d])	130 ± 3 (130−280[c])	142 ± 3 (260[d])
M210YA	104 ± 3	82 ± 3	95 ± 3	100 ± 3
M210YD	77 ± 7	54 ± 5	52 ± 5	59 ± 6
M210YF	88 ± 3	60 ± 2	58 ± 3	60 ± 3
M210YW[b]	128 ± 4	71 ± 3	70 ± 7	70 ± 7

[a]The shifts are given in wavenumbers (cm^{-1}). The calculated shifts for wild type, based on charges in a vacuum, are given in parentheses. [b]Note that in some of the slower mutants, such as M210YW, the initial reaction is significantly longer than wild type, and thus, there is slight mixing of $P^+H_A^-$ and $P^+Q_A^-$ at the peak of the shift; however, the value shown in the table should still represent a $P^+H_A^-$ population that is at least 70−80% pure [c]Calculated Stark shifts of B_A and B_B in the charge separated state $P^+H_A^-$ used the *Rb. sphaeroides* reaction center cystal structure; the values were adapted from ref 17. [d]Calculated Stark shifts of B_A and B_B in charge separaed state $P^+Q_A^-$ used the *Rb. sphaeroides* reaction center cystal structure; the values were adapted from ref 1.

as either due to the nuclear relaxation of B_A and B_B or attributed to the reaction heterogeneity of the reaction centers.[41,42] The faster decay of the B_A Stark shift is what one would expect if the protein was undergoing dielectric relaxation on roughly the same time scale as electron transfer, consistent with the previous suggestion that nuclear dynamics plays a role in the wavelength dependence of the H_A^- to Q_A reaction.[41,42] In this case, both the movement of the charge to Q_A and dielectric relaxation are decreasing the effective field felt by B_A simultaneously. As would be expected if the complex kinetics were associated with a response to electron transfer, all of the 100 ps dynamics are absent in Q_A-depleted reaction centers (see below).

In contrast with wild type, the B_A dynamic Stark shift in the M210YD mutant follows the electron-transfer kinetics quite well on this time scale, suggesting that the dielectric relaxation near B_A in this mutant does not take place on a time scale comparable to electron transfer in the mutant. It appears that the M210YD mutant alters the protein environment near B_A in such a way that the correspondence between the electron-transfer kinetics and the electric field strength felt by B_A is altered relative to wild type on both the picosecond and 100 ps time scale (the initial and subsequent electron-transfer reactions). What this suggests is that relatively small changes in protein structure near B_A can have very signficiant and time-dependent effects on the dielectric response of the environment, a parameter that evolution has likely optimized in the series of temporally distinct electron-transfer reactions that take place in this system.

Stark Shift Kinetics in B_A versus B_B. B_A and B_B serve distinctly different functions in the reaction center. While they are in nearly symmetric positions in the structure, only B_A is thought to be an electron-transfer intermediate in normal charge separation. B_B is likely involved with the interaction between P and the carotenoid during ^3P quenching;[43] it is not clear if it plays any other direct role in reaction center function. Past work has demonstrated that changing the environment around the monomomer bacteriochlorophylls or changing the characteristics of the ligands has a substantial effect on the symmetry of electron transfer, presumably by altering the static redox potential of one or the other cofactor.[44−47] Steffen et al. showed that when a steady-state population of $P^+Q_A^-$ is generated using continuous illumination at 1.5 K, the fields felt by B_A and B_B are very different.[1] In fact, they concluded that the effective dielectric constant on the A-side was 4.7, 3-fold greater than that on the B-side. The effective dielectric constants were determined by comparing the magnitude of the Stark shift observed for B_A and B_B to that expected in a field generated by a charge-separated state in vacuum. Vos et al. obtained a smaller value for the effective dielectric constant near B_A on the picosecond time scale at 15 K in the state $P^+H_A^-$ (2.3−3).

The effective dielectric constant is related to the polarizability of the environment, which can have both instantaneous and time-dependent components. At higher temperature, one would expect an increase in protein movement and thus an increase in the time-dependent aspect of the dielectric. Comparing the values of the Stark shifts for B_A in the states $P^+H_A^-$ and $P^+Q_A^-$ reported here and those reported in refs 1 and 17, respectively (Table 1), one can see that the $P^+H_A^-$ value is much lower than that seen by Vos et al. at cryogenic temperature (104 cm^{-1} in this work versus 220 cm^{-1} in the study of Vos et al.), while the $P^+Q_A^-$ value is about the same as that observed at low temperature (83 cm^{-1} here versus 77 cm^{-1} in the study of Steffen et al.). While absolute comparisons between shifts at room temperature and cryogenic temperatures are imperfect due to the different band shape structures and approaches for monitoring the band shift, this suggests that at room temperature, there is a larger effective dielectric constant in the state $P^+H_A^-$ than there is at low temperature. This is presumably due to a very rapid local dielectric response at room temperature that is not possible at low temperature. The fact that the shifts observed between room temperature and low temperature are more similar in the state $P^+Q_A^-$ suggests that the changes that occur rapidly at room temperature still take place at low temperature but more slowly.

Consistent with the results of Steffen et al., B_B undergoes a larger shift in the $P^+Q_A^-$ state than does B_A (1.7 fold in this study, 2.3 fold in Steffen et al.), in contrast to the significantly lower shift that would be expected in a vacuum calculation (a ∼30% smaller shift for B_B versus B_A is expected).[1] This is also in line with the earlier conclusion that there is a large difference between the dielectric environments of B_A and B_B in the state $P^+Q_A^-$. At room temperature, that difference is apparently also present at early times when the symmetry-breaking reaction takes place. Table 1 shows that in the state $P^+H_A^-$, the B_A shift is 5−6 fold lower than that predicted from published vacuum calculations (i.e., the dielectric constant is in the range of 5−6)[17] and 4−5 fold lower than similar calculations for the state $P^+Q_A^-$. The effective dielectric constant for B_B remains in the range of 1−2 in both states. Vos et al. determined a smaller effective dielectric constant in the vicinity of B_A at low temperature (2.3−3.0), consistent with restricted motion at that temperature, but did not determine the effective dielectric constant near B_B.

dx.doi.org/10.1021/jp4037843 | J. Phys. Chem. B 2013, 117, 11383−11390

The complete time dependences of the Stark shift of the B_A and B_B absorption bands are compared in Figure 3a for reaction centers from wild type and four M210 mutants. Looking at wild type, both B_A and B_B Stark shifts rise together as electron transfer takes place, and to about the same extent, but then, the two diverge on longer time scales. The relative behavior of the Stark shifts for the two cofactors can be seen more clearly in Figure 3b. The absolute values of the shifts differ by only 25% initially and remain essentially the same through the initial reaction and out to 20−30 ps. After that, the relative shift value of B_B increases compared to B_A.

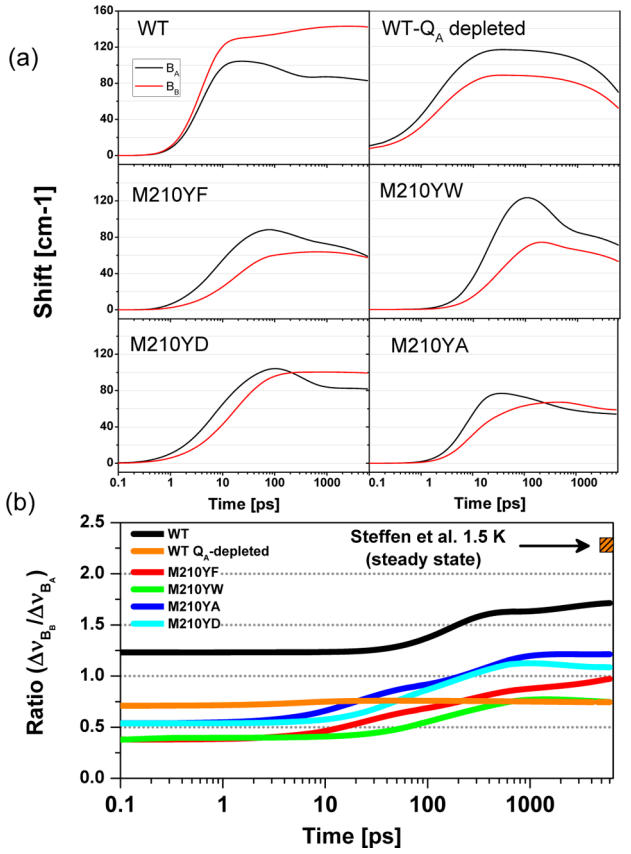

Figure 3. (a) Absorption band Stark shift kinetics of B_A (black lines) and B_B (red lines) for wild type and M210 mutants. The kinetics are constructed by the procedure described in the Materials and Methods section. (b) Time-dependent evolution of dynamic dielectric asymmetry after charge separation in wild type reaction centers (Q_A-containing and Q_A-depleted) and the M210 mutants. The dynamic dielectric asymmetry is expressed as a ratio of the dynamic Stark shift of accessory bacteriochlorophylls from two branches (B_B/B_A). Data are collected at room temperature over a 6 ns time window. The steady-state dielectric asymmetry at low temperature (1.5 K) from Steffen et al.[1] is shown as a shaded square.

The relative time dependence of the B_A and B_B Stark shifts described above reflects the kinetics (though not the absolute values) expected from vacuum field calculations (Table 1). Both fields rise upon initial charge separation. As electron transfer continues from H_A^- to Q_A, however, the field near B_A drops because the charge separation is over a longer distance, lowering the field strength at any point between the charges. The field near B_B continues to increase during electron transfer to Q_A because the charge-separated state looks less and less like a dipole and more like a single positive charge on P. The concept that it is the effect of the electron transfer to Q_A that distinguishes the time dependence of the B_A and B_B band shifts is supported by the fact that in quinone-depleted wild type reaction centers, the ratio of the Stark shifts associated with B_A and B_B becomes time-independent.

The kinetics of the B_B Stark shift are somewhat different in the mutants, primarily in that the development of this shift appears more spread out over time between about 10 and 100 ps, a considerably longer range than is observed for the shift in the B_A band (Figure 3a). As a result, the ratio of the shifts between B_B and B_A gradually increases on the time scale of the electron transfer to the quinone (Figure 3b). This is likely the result, at least in part, of the lengthened initial electron transfer in the mutants convolved with the continued increase in the B_B Stark shift over time, as seen in the wild type.

CONCLUSIONS

The time-dependent Stark shift associated with the monomer bacteriochlorophylls represents a useful way to monitor the effect and magnitude of dielectric relaxation during electron transfer. At room temperature, the effective dielectric constant remains in the 4−6 range near B_A and in the 1−2 range near B_B throughout the electron-transfer process forming $P^+Q_A^-$. The wavelength-dependent kinetics previously observed for the electron transfer from H_A^- to Q_A[41] can be explained in terms of dielectric relaxation and associated shifts in the ground-state spectrum of the monomer bacteriochlorophylls. Mutants known to alter the environment near B_A also alter the time dependence of the Stark shift.

ASSOCIATED CONTENT

Supporting Information

Transient absorption spectra at selected decay times; global fitting results (EADS and corresponding kinetics, obtained using a sequential kinetic model A → B → C → D → E); absolute absorption spectra using Gaussian fitting; and the estimation of errors of Stark shifts. This material is available free of charge via the Internet at http://pubs.acs.org.

AUTHOR INFORMATION

Corresponding Author

*E-mail: zhi.guo.29@nd.edu (Z.G.); nwoodbury@asu.edu (N.W.W.).

Notes

The authors declare no competing financial interest.

ACKNOWLEDGMENTS

This work was funded by NSF Grant MCB-0642260 and MCB-1157788. The authors thank Dr. Pan Jie for helpful discussions.

ABBREVIATIONS

Rb. sphaeroides	*Rhodobacter sphaeroides*
P	special pair of bacteriochlorophylls
B_A, B_B	monomeric bacteriochlorophylls
H_A, H_B	bacteriopheophytins
Q_A, Q_B	quinones
EADS	evolution-associated difference spectrum
ps	picosecond
ns	nanosecond

REFERENCES

(1) Steffen, M. A.; Lao, K.; Boxer, S. G. Dielectric Asymmetry in The Photosynthetic Reaction Center. *Science* **1994**, *264*, 810−816.

(2) Liptay, W. Dipole Moments and Polarizabilities of Molecules in Excited Electronic States. *Excited States* **1974**, *1*, 129−229.

(3) Liptay, W. Optical Absorption of Molecules in Liquid Solutions in an Applied External Electric Field (Electrochromism). *Ber. Bunsen-Ges. Phys. Chem* **1976**, *80*, 207−217.

(4) Lösche, M.; Feher, G.; Okamura, M. Y. The Stark Effect in Reaction Centers from Rhodobacter Sphaeroides R-26 and Rhodopseudomonas Viridis. *Proc. Natl. Acad. Sci. U.S.A.* **1987**, *84*, 7537−7541.

(5) Lockhart, D. J.; Boxer, S. G. Magnitude and Direction of The Change in Dipole Moment Associated with Excitation of the Primary Electron Donor in Rhodopseudomonas Sphaeroides Reaction Centers. *Biochemistry* **1987**, *26*, 664−668.

(6) Hammes, S. L.; Mazzola, L.; Boxer, S. G.; Gaul, D. F.; Schenck, C. C. Stark Spectroscopy of the Rhodobacter Sphaeroides Reaction Center Heterodimer Mutant. *Proc. Natl. Acad. Sci. U.S.A.* **1990**, *87*, 5682.

(7) Gottfried, D. S.; Steffen, M. A.; Boxer, S. G. Large Protein-Induced Dipoles for a Symmetric Carotenoid in a Photosynthetic Antenna Complex. *Science* **1991**, *251*, 662−665.

(8) Pierce, D. W.; Boxer, S. G. Stark Effect Spectroscopy of Tryptophan. *Biophys. J.* **1995**, *68*, 1583−1591.

(9) Bublitz, G. U.; Boxer, S. G. Stark Spectroscopy: Applications in Chemistry, Biology, and Materials Science. *Annu. Rev. Phys. Chem.* **1997**, *48*, 213−242.

(10) Bublitz, G.; King, B. A.; Boxer, S. G. Electronic Structure of the Chromophore in Green Fluorescent Protein (GFP). *J. Am. Chem. Soc.* **1998**, *120*, 9370−9371.

(11) Silverman, L. N.; Spry, D.; Boxer, S. G.; Fayer, M. Charge Transfer in Photoacids Observed by Stark Spectroscopy. *J. Phys. Chem. A* **2008**, *112*, 10244−10249.

(12) Fafarman, A. T.; Sigala, P. A.; Schwans, J. P.; Fenn, T. D.; Herschlag, D.; Boxer, S. G. Quantitative, Directional Measurement of Electric Field Heterogeneity in the Active Site of Ketosteroid Isomerase. *Proc. Natl. Acad. Sci. U.S.A.* **2012**, *109*, E299−E308.

(13) Labhart, H. Electrochromism. In *Advances in Chemical Physics*; John Wiley & Sons, Inc.: New York, 2007; pp 179−204.

(14) Krawczyk, S.; Daniluk, A. Solvent Effects and Vibrational Dependence in Electrochromic Spectra of Carotenoids. *Chem. Phys. Lett.* **1995**, *236*, 431−437.

(15) Chang, I. Electrochromic and Electrochemichromic Materials and Phenomena. *Nonemissive Electroopt. Disp.* **1976**, 155−96.

(16) Bolton, J. R.; Clayton, R. K.; Reed, D. W. An Identification of the Radical Giving Rise to the Light-Induced Electron Spin Resonance Signal in Photosynthetic Bacteria. *Photochem. Photobiol.* **1969**, *9*, 209−218.

(17) Vos, M. H.; Rischel, C.; Jones, M. R.; Martin, J.-L. Electrochromic Detection of a Coherent Component in the Formation of the Charge Pair P^+HL^- in Bacterial Reaction Centers. *Biochemistry* **2000**, *39*, 8353−8361.

(18) Kirmaier, C.; Holten, D. Primary Photochemistry of Reaction Centers from the Photosynthetic Purple Bacteria. *Photosynth. Res.* **1987**, *13*, 225−260.

(19) Woodbury, N.; Allen, J. The Pathway, Kinetics and Thermodynamics of Electron Transfer in Wild Type and Mutant Reaction Centers of Purple Nonsulfur Bacteria. *Anoxygenic Photosynthetic Bacteria* **2004**, 527−557.

(20) Lockhart, D. J.; Boxer, S. G. Stark Effect Spectroscopy of Rhodobacter Sphaeroides and Rhodopseudomonas Viridis Reaction Centers. *Proc. Natl. Acad. Sci. U.S.A.* **1988**, *85*, 107−111.

(21) Gottfried, D. S.; Stocker, J. W.; Boxer, S. G. Stark Effect Spectroscopy of Bacteriochlorophyll in Light-Harvesting Complexes from Photosynthetic Bacteria. *Biochim. Biophys. Acta* **1991**, *1059*, 63−75.

(22) Boxer, S. G. Stark Spectroscopy of Photosynthetic Systems. *Biophysical Techniques in Photosynthesis* **2004**, 177−189.

(23) Lao, K.; Moore, L. J.; Zhou, H.; Boxer, S. G. Higher-Order Stark Spectroscopy: Polarizability of Photosynthetic Pigments. *J. Phys. Chem.* **1995**, *99*, 496−500.

(24) Franzen, S.; Goldstein, R. F.; Boxer, S. G. Electric Field Modulation of Electron Transfer Reaction Rates in Isotropic Systems: Long Distance Charge Recombination in Photosynthetic Reaction Centers. *J. Phys. Chem.* **1990**, *94*, 5135−5149.

(25) Lockhart, D. J.; Kirmaier, C.; Holten, D.; Boxer, S. G. Electric Field Effects on The Initial Electron-Transfer Kinetics in Bacterial Photosynthetic Reaction Centers. *J. Phys. Chem.* **1990**, *94*, 6987−6995.

(26) Treynor, T. P.; Yoshina-Ishii, C.; Boxer, S. G. Probing Excited-State Electron Transfer by Resonance Stark Spectroscopy: 4. Mutations near BL in Photosynthetic Reaction Centers Perturb Multiple Factors that Affect $B_L^* \rightarrow B_L^+ H_L^-$. *J. Phys. Chem. B* **2004**, *108*, 13523−13535.

(27) Haffa, A. L. M.; Lin, S.; Katilius, E.; Williams, J. C.; Taguchi, A. K. W.; Allen, J. P.; Woodbury, N. W. The Dependence of the Initial Electron-Transfer Rate on Driving Force in Rhodobacter sphaeroides Reaction Centers. *J. Phys. Chem. B* **2002**, *106*, 7376−7384.

(28) Haffa, A. L. M.; Lin, S.; Williams, J. C.; Bowen, B. P.; Taguchi, A. K. W.; Allen, J. P.; Woodbury, N. W. Controlling the Pathway of Photosynthetic Charge Separation in Bacterial Reaction Centers. *J. Phys. Chem. B* **2003**, *108*, 4−7.

(29) Guo, Z.; Woodbury, N. W.; Pan, J.; Lin, S. Protein Dielectric Environment Modulates the Electron-Transfer Pathway in Photosynthetic Reaction Centers. *Biophys. J.* **2012**, *103*, 1979−1988.

(30) Goldsmith, J. O.; Boxer, S. G. Rapid Isolation of Bacterial Photosynthetic Reaction Centers With an Engineered Poly-histidine Tag. *Biochim. Biophys. Acta* **1996**, *1276*, 171−175.

(31) Okamura, M.; Isaacson, R.; Feher, G. Primary Acceptor in Bacterial Photosynthesis: Obligatory Role of Ubiquinone in Photoactive Reaction Centers of Rhodopseudomonas Spheroides. *Proc. Natl. Acad. Sci. U.S.A.* **1975**, *72*, 3491−3495.

(32) Snellenburg, J. J.; Laptenok, S. P.; Seger, R.; Mullen, K. M.; van Stokkum, I. H. Glotaran: A Java-Based Graphical User Interface for the R Package TIMP. *J. Stat. Software* **2012**, *49*, 1−22.

(33) Breton, J. *The Photosynthetic Bacterial Reaction Center: Structure and Dynamics*; Nato ASI Series A, Life Sciences; Springer: New York, 1988; Vol. *149*.

(34) McAuley, K. E.; Fyfe, P. K.; Cogdell, R. J.; Isaacs, N. W.; Jones, M. R. X-ray Crystal Structure of The YM210W Mutant Reaction Centre from *Rhodobacter Sphaeroides*. *FEBS Lett.* **2000**, *467*, 285−290.

(35) Nagarajan, V.; Parson, W.; Davis, D.; Schenck, C. Kinetics and Free Energy Gaps of Electron-Transfer Reactions in Rhodobacter Sphaeroides Reaction Centers. *Biochemistry* **1993**, *32*, 12324−12336.

(36) Beekman, L.; van Stokkum, I.; Monshouwer, R.; Rijnders, A.; McGlynn, P.; Visschers, R.; Jones, M.; van Grondelle, R. Primary Electron Transfer in Membrane-Bound Reaction Centers with Mutations at the M210 Position. *J. Phys. Chem.* **1996**, *100*, 7256−7268.

(37) Fyfe, P. K.; Jones, M. R. Re-emerging Structures: Continuing Crystallography of the Bacterial Reaction Centre. *Biochim. Biophys. Acta* **2000**, *1459*, 413−421.

(38) Wang, H.; Lin, S.; Allen, J. P.; Williams, J. A. C.; Blankert, S.; Laser, C.; Woodbury, N. W. Protein Dynamics Control the Kinetics of Initial Electron Transfer in Photosynthesis. *Science* **2007**, *316*, 747−750.

(39) LeBard, D. N.; Matyushov, D. V. Protein−Water Electrostatics and Principles of Bioenergetics. *Phys. Chem. Chem. Phys.* **2010**, *12*, 15335−15348.

(40) LeBard, D. N.; Kapko, V.; Matyushov, D. V. Energetics and Kinetics of Primary Charge Separation in Bacterial Photosynthesis. *J. Phys. Chem. B* **2008**, *112*, 10322−10342.

(41) Kirmaier, C.; Holten, D.; Parson, W. W. Temperature and Detection-Wavelength Dependence of the Picosecond Electron-Transfer Kinetics Measured in Rhodopseudomonas Sphaeroides Reaction Centers. Resolution of New Spectral and Kinetic Components in the Primary Charge Separation Process. *Biochim. Biophys. Acta* **1985**, *810*, 33−48.

(42) Kirmaier, C.; Holten, D. Evidence That a Distribution of Bacterial Reaction Centers Underlies the Temperature and Detection-Wavelength Dependence of the Rates of the Primary Electron-Transfer Reactions. *Proc. Natl. Acad. Sci. U.S.A.* **1990**, *87*, 3552−3556.
(43) Frank, H. A.; Violette, C. A. Monomeric Bacteriochlorophyll Is Required for the Triplet Energy Transfer between the Primary Donor and the Carotenoid in Photosynthetic Bacterial Reaction Centers. *Biochim. Biophys. Acta* **1989**, *976*, 222−232.
(44) Heller, B. A.; Holten, D.; Kirmaier, C. Control of Electron Transfer Between The L- and M-Sides of Photosynthetic Reaction Centers. *Science* **1995**, *269*, 940.
(45) Kirmaier, C.; Weems, D.; Holten, D. M-Side Electron Transfer in Reaction Center Mutants with a Lysine near the Nonphotoactive Bacteriochlorophyll. *Biochemistry* **1999**, *38*, 11516−11530.
(46) Chuang, J. I.; Boxer, S. G.; Holten, D.; Kirmaier, C. High Yield of M-Side Electron Transfer in Mutants of Rhodobacter Capsulatus Reaction Centers Lacking the L-Side Bacteriopheophytin. *Biochemistry* **2006**, *45*, 3845−3851.
(47) Carter, B.; Boxer, S. G.; Holten, D.; Kirmaier, C. Photochemistry of a Bacterial Photosynthetic Reaction Center Missing the Initial Bacteriochlorophyll Electron Acceptor. *J. Phys. Chem. B* **2012**, *116*, 9971−9982.